ADVANCED FUNCTIONAL MATERIALS
www.afm-journal.de

Highly Asymmetric, Interfaced Dimers Made of Au Nanoparticles and Bimetallic Nanoshells: Synthesis and Photo-Enhanced Catalysis

*Yongxing Hu, Yuzi Liu, Zheng Li, and Yugang Sun**

Synthesis of a class of exotic interfaced dimers with high asymmetries in terms of composition, morphology, structure (solid versus hollow), and dimension of the individual nanoscale components in the dimers is successfully accomplished. Typical examples include the interfaced dimers made of solid Au nanoparticles and hollow bimetallic nanoshells with different compositions, such as Au/Ag, Pt/Ag, and Pd/Ag. The success of the synthesis relies on the combination of asymmetric overgrowth of Ag nanodomains on the partially passivated Au nanoparticles and a following galvanic replacement reaction between the Ag nanodomains and appropriate noble metal precursors. The entire synthesis is processed on the unique superparamagnetic colloidal substrates that offer many advantages, such as time-efficiency, scalability, and high yield. The Au nanoparticle and the bimetallic nanoshell in each interfaced dimer are in direct contact, resulting in the possible strong coupling between them as well as novel properties that cannot be observed in either the nanoparticle or the nanoshell. For example, dimers made of Au nanoparticles and Pd/Ag nanoshells exhibit enhanced catalytic performance toward Suzuki coupling reactions under illumination of visible light because the strong surface plasmon resonances in the Au nanoparticles can influence the catalytic activity of the Pd/Ag nanoshells through coupling between the nanoparticles and the nanoshells.

1. Introduction

Noble metal nanostructures have attracted enormous interest because of their novel properties and corresponding applications in a broad range of areas, such as catalysis, sensing, surface enhanced spectroscopy, biological imaging, optoelectronics, etc.[1–5] For example, nanoparticles made of gold (Au) and silver (Ag) represent a class of strong optical absorbers and substrates for surface enhanced Raman scattering (SERS).[6,7] They exhibit interesting optical properties due to their strong surface plasmon resonances (SPRs) that strongly depend on their sizes and morphologies.[8,9] Nanoparticles made of platinum (Pt), palladium (Pd), and their alloys have been demonstrated to be efficient catalysts for many different reactions such as fuel cell reactions, water splitting reactions, etc. by taking the advantages of their large surface-to-volume ratios and shaped-dependent specific crystallographic surfaces.[10–14] Great success has been achieved in the synthesis of noble metal nanoparticles with well-controlled compositions and morphologies in the last decade due to the extensive efforts in many groups.[15–18] However, synthesis of hybrid dimers made of noble metal nanostructures with asymmetric configurations in terms of geometries and compositions is still challenging but attractive as the coupling between different components in the hybrid nanostructures may lead to novel properties and applications.[19–21] For instances, dimers made of either equivalent plasmonic nanoparticles (homodimers) or non-equivalent nanoparticles (heterodimers) have been demonstrated to be a class of promising SERS substrates due to the creation of hot spots between the individual nanoparticles in each dimer.[22,23] Up till now, most synthesis of nanoparticle dimers are accomplished through controlled assembly of individual nanoparticles with appropriate compositions and morphologies.[24] The most straightforward strategy is linking two nanoparticles together to form a dimer, which relies on the modification of the nanoparticle surfaces with appropriate molecules that can bind nanoparticles together. Research groups led by Alivisatos, Mirkin, and Gang have pioneeringly demonstrated the use of DNA molecules to link Au nanoparticles into dimers through the specific hybridization of the complementary single-stranded DNA molecules on different nanoparticles.[25–28] Most recently, carefully decreasing the stability of colloidal nanoparticles has been demonstrated to be an alternative approach that enables the spontaneous aggregation of individual nanoparticles to form dimers. Examples include lowering stability of colloidal Ag nanoparticles capped with poly(vinylpyrrolidone) (PVP) by slightly etching them with $Fe(NO_3)_3$,[29] adding HCl to citrate-stabilized Au nanoparticles,[30] and tuning the hydrophobicity of solvents for amphiphilic Au nanoparticles capped with both hydrophilic and hydrophobic polymers.[31,32] In these

Dr. Y. Hu, Dr. Y. Liu, Dr. Z. Li, Dr. Y. Sun
Center for Nanoscale Materials
Argonne National Laboratory
9700 South Cass Avenue , Argonne, IL, 60439, USA
E-mail: ygsun@anl.gov

DOI: 10.1002/adfm.201303557

examples, surface chemistry of individual nanoparticles is uniform and the surface of each nanoparticle can be potentially accessed by multiple nanoparticles, leading to an increased possibility for the formation of aggregates with more than two nanoparticles (e.g., trimmers, tetramers, etc.) that exhibit higher geometric symmetry than dimers. In order to increase the yield of nanoparticle dimers, "patchy surfaces" with non-uniform chemistries (or properties) are necessary to be created in the precursor nanoparticles to provide an anisotropic surface environment that can assist the assembly (and/or growth) of nanoparticles into asymmetric dimers.[33–37] For example, physically embedding partial surfaces of Au nanoparticles in an inert matrix (e.g., SiO_2, polymers) enables modification of the partially exposed Au nanoparticle surfaces with desirable molecules that can specifically bind other nanoparticles to form nanoparticle dimers.[25,38] From the Au nanoparticles with partially passivated surfaces, interfaced dimers made of two directly contacted metal nanodomains can also be synthesized through the epitaxial overgrowth of Ag (or Au) over the partial unpassivated Au surfaces.[39,40]

In this work, we report that interfaced asymmetric dimers made of even more complex compositions and geometries can be synthesized by combining the controlled synthesis of interfaced dimers and nanoscale galvanic replacement reactions. Typical examples include interfaced dimers made of solid Au nanoparticles and hollow bimetallic nanoshells of different compositions (e.g., Au/Ag, Pt/Ag, Pd/Ag). The composition, size, configuration (e.g., single-layered or double-layered) of the metal nanoshells as well as the overlap between the Au nanoparticles and the metal nanoshells can be tuned by controlling the synthesis conditions. Due to the formation of direct interfaces between the Au nanoparticles and the bimetallic nanoshells, strong coupling between these two components in each dimer is expected to possibly induce novel properties that cannot be observed in any singe components.

2. Results and Discussion

The major steps involved in the synthesis of asymmetric, interfaced dimers made of solid Au nanoparticles (Au NPs) and hollow bimetallic nanoshells are highlighted in **Figure 1**. The superparamagnetic Fe_3O_4-SiO_2 core–shell nanoparticles are used as colloidal substrates that serve as a unique class of platform for large-scale synthesis of complex nanostructures. The SiO_2 surfaces of the core–shell nanoparticles can be modified with 3-aminopropyl-triethoxysilane (APTS) molecules by incubating the colloidal nanoparticles with APTS at a mild temperature (e.g., 80 °C) due to the formation of siloxane (-Si-O-Si-) bonds.[41] The amino groups at the ends of the APTS molecules expose to the surrounding solution. Mixing the APTS-modified Fe_3O_4-SiO_2 core–shell nanoparticles with the citrate-stabilized Au NPs (i.e., Au seeds) leads to the attachment of the Au seeds to the core-shell nanoparticles by the strong chemical affinity between Au atoms and N atoms in the amino groups (Step I). Based on the difference in surface chemistry between the SiO_2 shells and the Au seeds, a second layer of SiO_2 can be selectively deposited on the original SiO_2 shells when applying a modified Stöber reaction.[38] By controlling the thickness of the second SiO_2 layer, the Au seeds can be partially embedded

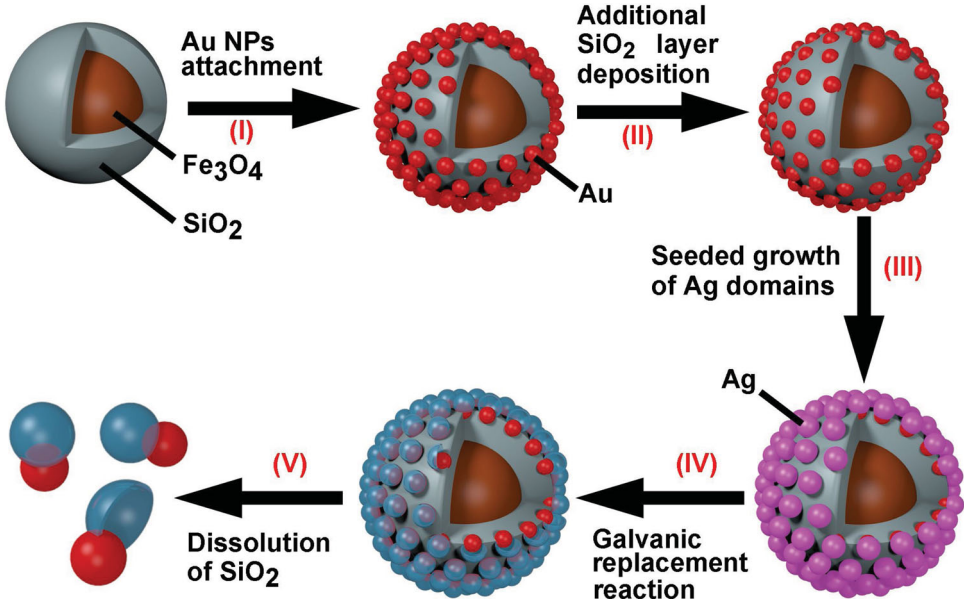

Figure 1. Schematic illustration of the major steps involved in the synthesis of interfaced dimers made of Au NPs and bimetallic nanoshells: I) seeding of Au nanoparticles on the surface of a superparamagnetic Fe_3O_4-SiO_2 core–shell colloidal substrate through chemical adsorption of Au nanoparticles to the amino groups pre-grafted on the SiO_2 surface; II) selective deposition of a second SiO_2 layer on the original SiO_2 shell, resulting in partial embedding of the Au seeds in a SiO_2 matrix; III) epitaxial overgrowth of Ag domains on the exposed surfaces of the Au seeds due to same crystalline lattice structure and very close lattice constants in Au and Ag nanocrystals; IV) galvanic replacement reaction over the Ag domains with appropriate noble metal precursors, enabling a transformation of the Ag domains to bimetallic hollow nanoshells; V) release of the interfaced Au NP-bimetallic nanoshell dimers from the colloidal substrate by dissolving the SiO_2 layer in a basic solution.

in the SiO_2 matrix, leaving a portion of their pristine surfaces accessible to the surrounding solution (step II, see the example shown in Figures S1a,b, Supporting Information). Partially embedding the Au seeds by SiO_2 matrix is important in two folds: i) the Au seeds can be strongly immobilized on the colloidal substrates to avoid the potential detachment in the following synthetic steps; and ii) it provides locally asymmetric environment on Au seeds for anisotropically seeded growth of Ag domains. The exposed surfaces of the Au seeds act as nucleation sites for the overgrowth of Ag domains, generating asymmetric, interfaced dimers made of solid Au and Ag nanodomains on the Fe_3O_4-SiO_2 colloidal substrates (step III, see example shown in Figures S1c,d, Supporting Information). The size of Ag domains can be tuned by controlling the concentration of $AgNO_3$ in the plating solution. As reported in the previous work, the Ag nanodomains can be transformed to hollow bimetallic nanoshells through the conventional galvanic replacement reactions between the Ag nanodomains and noble metal precursors with high oxidation states (e.g., $AuCl_4^-$, $PdCl_4^{2-}$, $PtCl_4^{2-}$).[42] By adding an appropriate metal precursor, it produces asymmetric, interfaced dimers made of solid Au NPs (i.e., the Au seeds) and bimetallic hollow nanoshells that are attached to the Fe_3O_4-SiO_2 colloidal substrates (step IV). Dissolving the SiO_2 layer with NaOH solution can release the interfaced nanoparticle-nanoshell dimers from the Fe_3O_4-SiO_2 colloidal substrates (step V). The remaining superparamagnetic Fe_3O_4 nanoparticles can be easily separated with the assistance of an external magnetic field and be reused to start a new cycle of synthesis. The inclusion of the Fe_3O_4-SiO_2 nanoparticles as colloidal substrates is advantageous for the synthesis of highly asymmetric dimers in an efficient way. For instance, separation of the target nanoparticles from the precursor materials can be easily achieved by placing a magnet near the synthesis solution.

Reaction of the Ag nanodomains formed at step III (Figure 1) with an aqueous solution of $HAuCl_4$ at boiling temperature transforms the Ag nanodomains to Au/Ag alloy nanoshells with hollow interiors. Depending on the amount of $HAuCl_4$, the walls of the Au/Ag nanoshells exhibit different morphologies and different compositions.[43] In general, more $HAuCl_4$ facilitates the formation of Au/Ag nanoshells with porous walls due to the extended dealloying of the Au/Ag nanoshells. **Figure 2** presents the SEM images of an example of Au NP-Au/Ag nanoshell dimers obtained through such a galvanic replacement reaction. These dimers are still attached to the Fe_3O_4-SiO_2 colloidal substrates through the partially embedded Au NPs in the SiO_2 matrix. The dark contrast in the center of each Au/Ag nanoshell in the SEM images confirms their hollow interior. The wall of each Au/Ag nanoshell is not continuous and has small holes (Figure 2c). The solid Au NP (i.e., the Au seed) in each dimer is partially enclosed in the Au/Ag alloy nanoshell (highlighted by the arrows in Figure 2b). The corresponding TEM images (Figures S1e,f, Supporting Information) show the weaker contrast of the porous nanoshell than the solid Au NP, revealing the thin wall thickness of the nanoshell. The size and number of holes in the wall of each nanoshell may vary depending on the amount of $HAuCl_4$ used in the galvanic replacement reaction. TEM images in Figure S2 (Supporting Information) highlight the morphological evolution of the Au/Ag alloy nanoshells during the galvanic replacement reactions

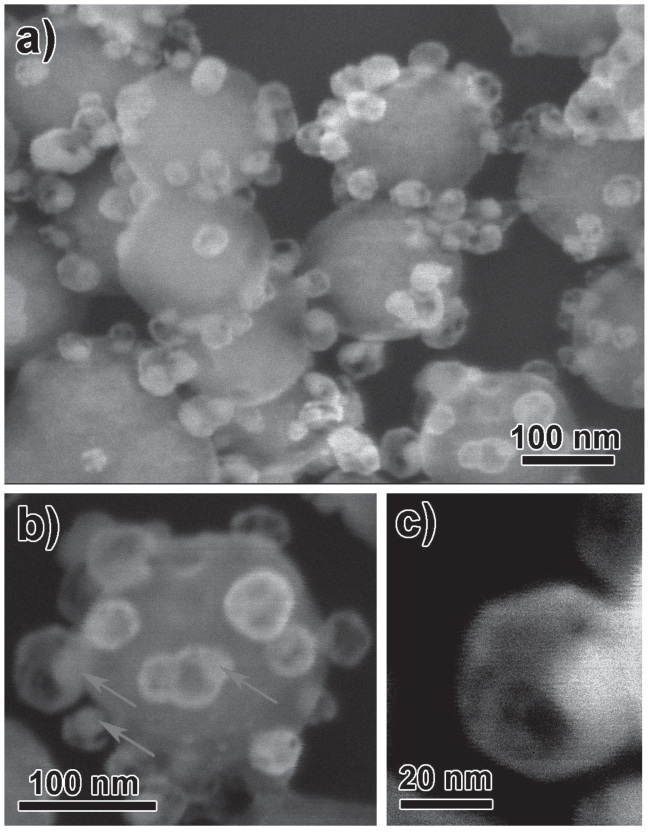

Figure 2. a) Typical SEM image of the interfaced dimers made of Au NPs and Au/Ag nanoshells on Fe_3O_4-SiO_2 colloidal core–shell particles. They were synthesized through the galvanic replacement reaction of the Fe_3O_4-SiO_2-Au-Ag composite particles shown in Figure S1c (Supporting Information) and an aqueous solution of $HAuCl_4$ at 100 °C. b) Enlarged SEM image of a single Fe_3O_4-SiO_2 colloidal particle, on which multiple interfaced Au NP-Au/Ag nanoshell dimers were formed. The arrows highlight the solid Au nanoparticles in the corresponding dimers. c) High-magnification SEM image of a single Au NP-Au/Ag nanoshell dimer.

with different amount of $HAuCl_4$, which is consistent with the previous report on mechanistic studies.[43] At the initial stage, only a small hole is formed on each Ag nanodomain due to the etching of the Ag with $AuCl_4^-$ ions. Continuous reaction dissolves more Ag, resulting in the formation of a hollow interior. The hole in the Ag nanodomain enables the Ag^+ ions diffuse out of the hollow interior to enlarge the hollow interior and the Au atoms generated from the galvanic reaction are deposited on the outside surfaces of the Ag nanodomain. Due to the high reaction temperature (i.e., ≈100 °C), the deposited Au atoms alloy with the underneath Ag nanodomain to form Au/Ag alloy nanoshell. When more Ag atoms are dissolved, the wall of the nanoshell becomes thinner and more holes are formed. As a result, the porosity and wall thickness of the Au/Ag alloy nanoshells in the asymmetric dimers can be tuned by controlling the reaction conditions. In addition, the size of the Au/Ag alloy nanoshells can also be tuned by growing the Ag nanodomains with different sizes in step III, Figure 1 (Figure S3, Supporting Information).

The asymmetric dimers composed of Au NPs and Au/Ag alloy nanoshells can be released from the colloidal substrates

by dissolving the SiO_2 layer with an aqueous solution of NaOH. The Fe_3O_4 cores can be easily removed with the assistance of a magnetic field, leaving a dispersion of pure dimers (**Figure 3**a). Each asymmetric dimer consists of a solid Au NP (with size of ≈15 nm) and a porous nanoshell, which are partially overlapped (Supporting Information, Movie S1). The wall thickness of the nanoshells is about 3 nm and the maximum lateral diameter of the nanoshell is about 35 nm. The overlap ratio between the solid Au NPs and the Au/Ag alloy nanoshells depends on how much the Au seeds are embedded in the SiO_2 matrix at step II, Figure 1. It is worth pointing out that the position of some solid Au nanoparticles is completely inside the nanoshells in the 2D projection TEM image shown in Figure 3a. This observation is due to the random orientations of the asymmetric dimers relative to the electron beam. For instance, a concentric core–shell projection profile can be observed when the electron beam is parallel to or close to the common axis (i.e., longitudinal axis) of a dimer. Figure 3b highlights the enlarged TEM image of two differently oriented asymmetric dimers. One stands on the carbon film with the Au nanoparticle sitting on the top of the nanoshell, giving a core–shell projection profile. The other lies on the TEM grid with its longitudinal axis parallel to the surface of the TEM grid, showing an asymmetric dimer profile. High-resolution TEM (HRTEM) images in Figure 3c,d reveal that the lattice fringes in the nanoshells continuously extend to the solid Au nanoparticles, indicating an epitaxial relationship between the Au NPs and the Au/Ag alloy shells. The elemental distributions of Au and Ag in the asymmetric dimers are characterized by energy dispersive X-ray (EDX) spectroscopy. The elemental concentration profiles (Figure 3f) along the arrowed line in Figure 3e clearly show the asymmetric distribution of both Au and Ag in the dimer. The line-scan profiles also reveal that the porous nanoshell is composed of Au and Ag with a hollow interior and the solid nanoparticle is composed of essentially pure Au. The results shown in Figures 2, 3 indicate that the dimers made of solid Au NPs and hollow Au/Ag alloy nanoshells exhibit asymmetry in term of both geometrical and compositional distributions.

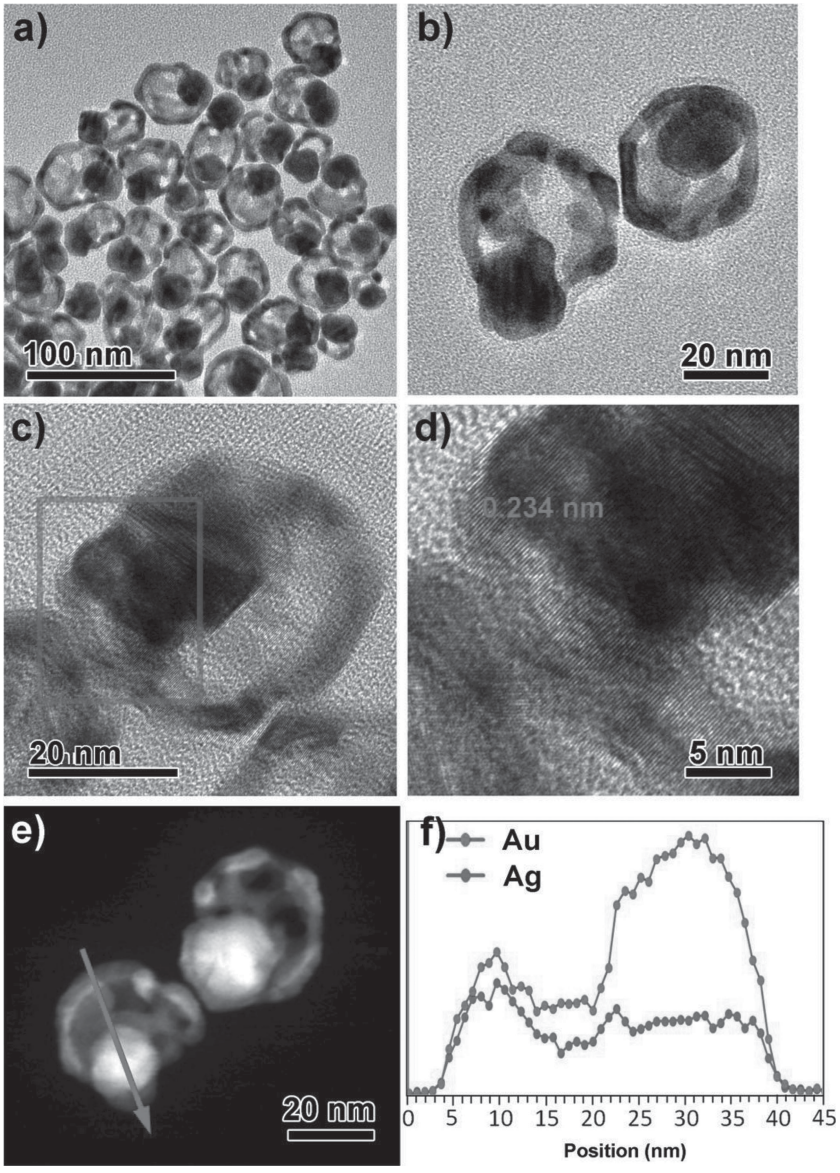

Figure 3. Characterization of the freestanding Au NP-Au/Ag nanoshell dimers that were released from the Fe_3O_4-SiO_2 colloidal substrates. a) Typical TEM image of random assembly of the interfaced dimers on a TEM grid. b) TEM image of two dimers, highlighting how the orientation of a dimer against the surface of TEM grid influences the two-dimensional projection profile of the dimer in the corresponding TEM image. Detailed explanation can be found in the text. c,d) High-resolution TEM images of an individual dimer, showing the directly contacted interface between the Au NP and the Au/Ag nanoshell. The continuous lattice fringes across the interface indicate the epitaxial relationship between the Au NP and the Au/Ag nanoshell. The image of frame (d) corresponds to the area highlighted by the rectangular box shown in (c). The interplanar distance measured from the adjacent lattice fringes in (d) is 0.234 nm, matching well with the (111) crystalline planes of face-centered cubic Au and Ag. e) Scanning transmission electron microscopy (STEM) image of two dimers sitting on a TEM grid with their longitudinal axes perpendicular to the electron beam. f) Distribution profiles of Au and Ag in one dimer along the arrowed line shown in (e). The results were determined from EDX spectral analysis. The electron beam was scanned along the line by following the arrowed direction. The top and bottom curves correspond to Au and Ag, respectively.

The complexity of the asymmetric dimers can be increased by repeating the steps III and IV in Figure 1 before the dimers are released from the Fe_3O_4-SiO_2 colloidal substrates. As shown in **Figure 4**a, asymmetric structures made of Au NPs and Au/Ag alloy double nanoshells can be synthesized through this strategy. An additional Ag layer is deposited on the surface of the existed Au/Ag alloy nanoshells by repeating the seeded growth process in step

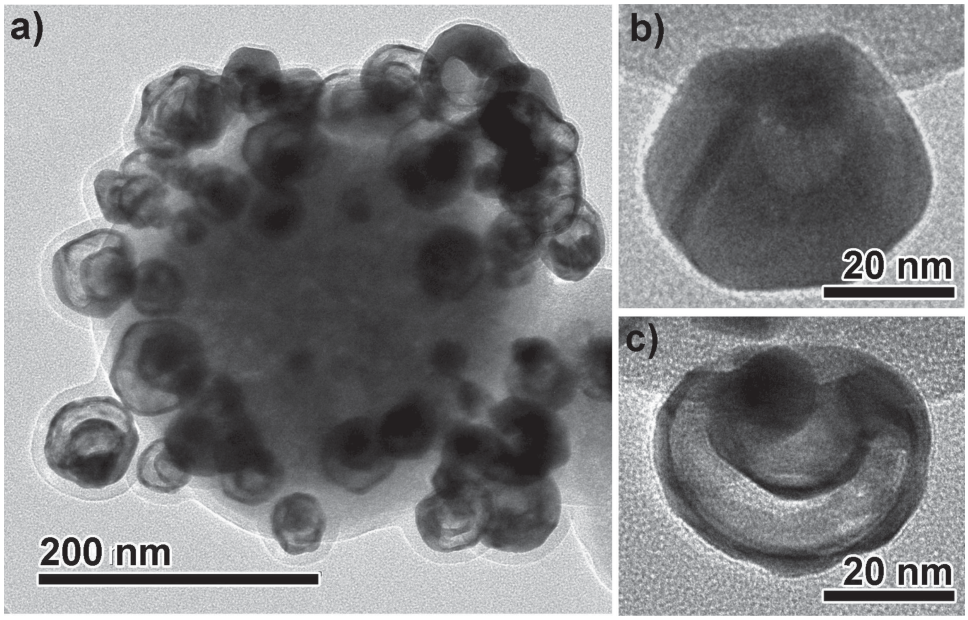

Figure 4. a) Typical TEM image of interfaced, asymmetric dimers made of Au NPs and double-layered Au/Ag nanoshells that were still on a Fe_3O_4-SiO_2 colloidal substrate. b) TEM image of an individual dimer consisting of an Au NP and an Au/Ag nanoshell after a thick layer of Ag was deposited on the Au/Ag nanoshell shown in Figure 3 through an electroless deposition. c) TEM image of an individual dimer with an Au NP and an Au/Ag double-layered nanoshell that was formed through galvanic replacement reaction between the dimer shown in (b) and an aqueous solution of $HAuCl_4$ at 100 °C.

III, Figure 1. The hollow interiors of the original nanoshells are preserved, as differentiated by the lighter contrast in the center of the metallic nanostructures (Figure 4b). The freshly deposited Ag layers are transformed into new Au/Ag alloy nanoshells after a second galvanic replacement with an aqueous solution of $HAuCl_4$ in step IV, Figure 1. The newly formed larger Au/Ag nanoshells enclose the original Au/Ag nanoshells, showing the double-walled feature. The Au NPs are still partially overlapped with the double-walled nanoshells (Figure 4c). If the precursors are different in the first and second galvanic replacement reactions with Ag, the compositions of each individual shell in a double-walled nanoshell can be different. The gap between the two walls in each double-walled nanoshell can also be tuned by controlling the thickness of the Ag layer deposited on the original Au/Ag alloy nanoshell in Figure 2. In principle, the processes of step III and IV in Figure 1 can be further repeated to form asymmetric dimers made of solid Au nanoparticles and multiple-walled bimetallic nanoshells.

The composition of the bimetallic nanoshells in the asymmetric dimers can be tuned by using different precursors to react with the Ag nanodomains at step IV, Figure 1. The product shown in **Figure 5**a represents an example of asymmetric dimers made of solid Au NPs (with size of ≈15 nm) and Pt/Ag bimetallic nanoshells (with size of ≈25 nm). An aqueous solution of Na_2PtCl_4 has been used as the precursor for galvanic replacement reaction. Different from the smooth surfaces of the Au/Ag alloy nanoshells shown in Figures 3–4, the surfaces of the Pt/Ag bimetallic nanoshells are rough. The difference in surface roughness might result from the different reaction rate in the galvanic replacement reactions. EDX spectra (Figure 5b) and line-scan analysis (Figure S4, Supporting Information) of individual dimers clearly show that the rough nanoshells are

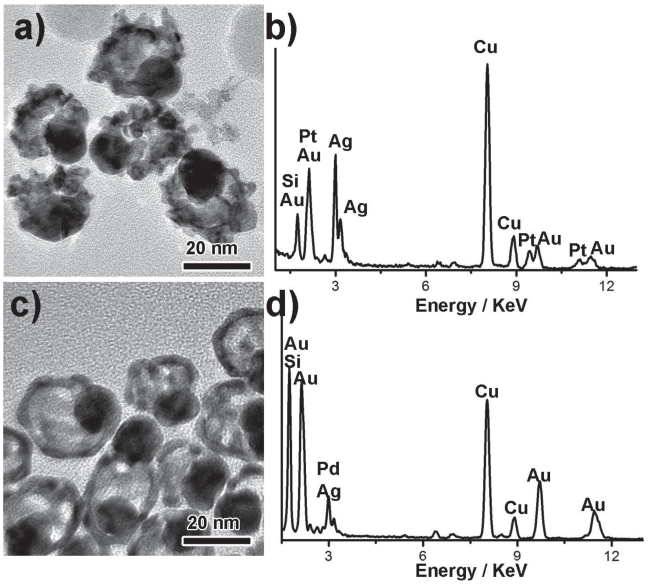

Figure 5. a) Typical TEM image of the asymmetric dimers made of Au NPs and Pt/Ag bimetallic nanoshells that were randomly assembly on a TEM grid. b) EDX spectrum taken from the dimers shown in (a). c) Typical TEM image and d) the corresponding EDX spectrum of the dimers made of Au NPs and Pd/Ag bimetallic nanoshells.

composed of both Pt and Ag. The strong signals of Au and Cu correspond to the solid Au NPs in the asymmetric dimers and the TEM grid, respectively. The signal of possible Si might originate from the detector. In addition, asymmetric dimers made of solid Au NPs and Pd/Ag bimetallic nanoshells (Figure 5c) are also achieved by using an aqueous solution of Na_2PdCl_4 as the

precursor in the galvanic replacement reaction. The representative EDX spectra (Figure 5d) and the elemental distribution analysis by energy-filtered TEM (Figure S5, Supporting Information) of individual dimers also confirm that the nanoshells in the asymmetric dimers are composed of Pd and Ag. The tunability in the composition of the nanoshells provides the opportunity to optimize the properties and functionalities of the synthesized asymmetric dimers. For example, optical absorption spectra of the dimers containing different nanoshells of Au/Ag, Pt/Ag, and Pd/Ag are compared in Figures S6–S8 (Supporting Information). The spectra clearly indicate that the Au NP-bimetallic nanoshell dimers exhibit similar extinction peaks around 520 nm corresponding to the SPRs of the Au NPs regardless of the composition of the nanoshells. The difference can be observed at wavelengths longer than 650 nm. The Au NP-Au/Ag nanoshell dimers exhibit a strong broad peak at ≈900 nm while both the Au NP-Pd/Ag nanoshell dimers and the Au NP-Pt/Ag nanoshell dimers only exhibit featureless tails with relatively lower intensity.

Among these bimetallic nanoshells, the Pd/Ag bimetallic nanoshells in the asymmetric dimers can be used as catalysts for Suzuki coupling reactions under elevated temperatures.[44,45] Conventional catalysts for the Suzuki coupling reactions are Pd based materials including two categories, that is, homogeneous catalysts (such as Pd complexes) and heterogeneous catalysts (such as nanoparticles containing Pd). Homogeneous catalysts usually suffer from the difficulty in recyclability although they exhibit better activity and selectivity than heterogeneous catalysts.[46] Nanoparticles made of pure Pd and bimetallic or multi-metallic nanoparticles containing Pd have also been developed to be used as attractive heterogeneous catalysts for Suzuki coupling reactions. The composite nanoparticles with multiple metals can be orders of magnitude cheaper than the nanoparticles made of pure Pd.[47] In the Au NP-Pd/Ag nanoshell asymmetric dimers shown in Figure 5c the Au NPs can serve as the light-harvesting center since they possess large extinction cross sections.[48,49] The asymmetric dimers allow the light energy harvested by the plasmonic component (i.e., Au NPs) to be utilized by the catalytic component (i.e., Pd/Ag nanoshells). Excited surface plasmon resonances (SPRs) can greatly enhance the electric fields near the surfaces of the Au NPs. The energetic or hot electrons upon plasmon excitation cool down through electron-phonon interactions, resulting in a rise of the lattice temperature in the metal. This thermal energy is then dissipated to the surrounding medium, causing the plasmonic photothermal conversion.[50,51] The plasmonic photothermal effect can accelerate chemical reactions on the catalytic Pd/Ag because reaction rates are dependent exponentially on temperature.[52] Therefore, the catalytic performance can be improved under photo-illumination when the Pd based catalysts are integrated with plasmonic nanocomponents, such as Au NPs.[53] The influence of light on the catalytic activity of the synthesized Au NP-Pd/Ag nanoshell dimers shown in Figure 5c has been evaluated. To avoid the serious aggregation of the dimers, the asymmetric dimers remain on the Fe_3O_4-SiO_2 colloidal substrates during the Suzuki coupling reactions. The extinction spectrum of the asymmetric dimers (Figure 5c) exhibits a broadband absorption in the visible range (Figure S6, Supporting Information) due to the strong SPRs in the Au NPs. As a result, Suzuki coupling reactions can be accelerated with the use of Au NP-Pd/Ag nanoshell dimers under illumination of visible light. In our experiment, the coupling reaction between phenylboronic acid and iodobenzene is catalyzed by the Au NP-Pd/Ag nanoshell dimers at 80 °C, resulting in the formation of biphenyl. Conversion of 95% reactants in the dark takes 45 min while no apparent reaction can be observed in the absence of the synthesized asymmetric dimers. In contrast, conversion of 95% reactants can be achieved within 15 min when the reaction is performed under illumination of visible light (**Figure 6**), indicating that SPR-based absorption of light can enhance the catalytic performance of Pd/Ag nanoshells in the Suzuki coupling reactions. To further confirm the Au NP's SPR enhancement on the visible light absorbance and thus the catalytic performance, absorption spectra of the Au NP-Pd/Ag nanoshell dimers and the freestanding Pd/Ag nanoshells (Figure S9, Supporting Information) are compared in Figure S10 (Supporting Information). The Au NP-Pd/Ag nanoshell dimers exhibit stronger absorbance in visible region with a peak at ≈520 nm that originates from the SPR of the Au NPs in comparison with the Pd/Ag nanoshells. In combination with the observed acceleration of reaction rate in the Suzuki coupling reactions catalyzed with the Au NP-Pd/Ag nanoshell dimers under photo-illumination, we can easily conclude that strong absorption of visible light in the Au NPs is responsible for the photo-enhanced catalytic performance highlighted in Figure 6. The photo-enhanced catalysis can shorten reaction time and thus save thermal energy used for driving the Suzuki coupling reactions.

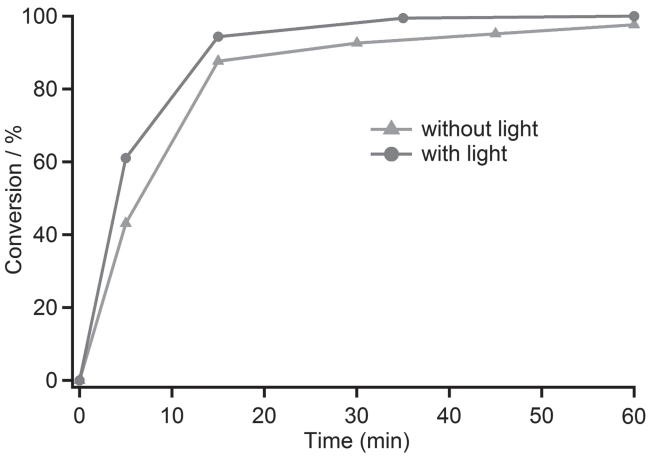

Figure 6. Conversion of iodobenzene in the Suzuki coupling reaction as a function of reaction time. The as-synthesized dimers composed of Au NPs and Pd/Ag nanoshells on the Fe_3O_4-SiO_2 colloidal substrates were used as catalysts. The profiles labeled with triangles and circles correspond to the reactions performed in the dark and under illumination of visible light, respectively.

3. Conclusions

In conclusion, we have developed an efficient approach for synthesizing highly asymmetric, interfaced dimers made of Au NPs and bimetallic nanoshells that are difficult (or impossible)

to achieve via the conventional methods reported in literature. The synthesis relies on the combination of 1) growing interfaced Au NP-Ag NP dimers on the superparamagnetic colloidal substrates and 2) reacting the Ag NPs in the dimers with noble metal precursors (e.g., $HAuCl_4$, Na_2PtCl_4, Na_2PtCl_4) to transform the Ag NPs into bimetallic hollow nanoshells via the nanoscale galvanic replacement reactions. By taking advantages of the tuning flexibility of reaction conditions in the multiple steps in Figure 1, the interfaced Au NP-bimetallic nanoshell dimers can be easily controlled in terms of compositions, dimensions, geometries, and configurations, thus enabling the ability to tailor the properties of the synthesized dimers. The direct contact between the Au NPs and the bimetallic nanoshells in the interfaced dimers is beneficial for strong coupling between the NPs and nanoshells to induce unique properties and potential applications.[54] For example, the Au NP-Pd/Ag bimetallic nanoshell dimers can be used to catalyze classical Suzuki coupling reactions on the surfaces of the Pd/Ag nanoshells. The strong SPRs in the Au NPs enables absorption of visible light in the dimers, leading to an enhancement in catalytic performance under photo-illumination due to the coupling of the unique optical properties of the Au NPs and the catalytic properties of the Pd/Ag nanoshells.

4. Experimental Section

Chemicals: Denatured ethanol, isopropanol (99.9%), ammonium hydroxide aqueous solution (28 wt%) and sodium hydroxide pallets (A.C.S. grade) were purchased from Fisher Scientific. 3-Aminopropyl-triethoxysilane (APTS, 99%), potassium iodide (KI), and poly(vinylpyrrolidone) (PVP) K12 ($M_w \approx 3500$) were obtained from Acros Organics. Poly (acrylic acid) (PAA, $M_w \approx 1800$), tetraethyl orthosilicate (TEOS, 98%), hydrogen tetrachloroaurate(III) trihydrate ($HAuCl_4 \cdot 3H_2O$, 99.9+%), sodium citrate tribasic dihydrate (99%), silver nitrate ($AgNO_3$, ≥99.0%), acetonitrile (anhydrous, 99.8%), diethylene glycol (DEG), L-ascorbic acid, sodium tetrachloroplatinate(II) hydrate ($Na_2PtCl_4 \cdot H_2O$), sodium tetrachloropalladate(II) (Na_2PdCl_4, 98%), hexanes (HPLC grade, >95%), phenylboronic acid (95%), and iodobenzene (98%) were purchased from Sigma-Aldrich. PVP K15 ($M_w \approx 10000$) was purchased from Fluka. All chemicals were used as received without further purification and treatment.

Synthesis of Fe_3O_4-SiO_2 Core–Shell Particles Decorated with Au Nanoparticles: The synthesis followed the processes developed previously.[38] In a typical synthesis, a controlled hydrolysis and partial reduction of $FeCl_3$ in a basic diethylene glycol (DEG) solution containing NaOH and PAA at 220 °C was firstly carried out to generate superparamagnetic Fe_3O_4 nanoparticles with an average diameter of 155 nm.[55] The Fe_3O_4 nanoparticles were then coated with a SiO_2 layer through a modified Stöber reaction.[56] To a mixture including aqueous dispersion of Fe_3O_4 nanoparticles (≈23 mg Fe_3O_4, 3 mL) and ethanol (20 mL) was added ammonium hydroxide aqueous solution (1 mL), followed by an injection of TEOS (0.1 mL) to initiate the deposition of silica on the surfaces of the Fe_3O_4 nanoparticles. After the reaction lasted 20 minutes, the resulting Fe_3O_4-SiO_2 core–shell particles were collected with the assistance of an external magnetic field and were washed with ethanol twice to remove the chemical species adsorbed on the silica layer. Incubating the core–shell particles in isopropanol (20 mL) containing APTS (50 µL) at 80 °C for 2 h led to the modification of the surfaces of the silica shells with amino groups from APTS molecules.[38] The modified particles were later concentrated with an external magnetic field, washed with isopropanol and deionized (DI) water, and re-dispersed in DI water (3 mL). Note: The Fe_3O_4-SiO_2 particles were very stable and well dispersed in isopropanol due to the abundant hydroxyl groups on the surface of SiO_2 shells that made the particle surfaces to be compatible with isopropanol.[56] Similarly, the Fe_3O_4-SiO_2 particles also exhibited high stability during the decoration of particle surfaces with APTS due to the compatibility between amino groups of APTS and isopropanol molecules. As a result, no particle aggregation was observed throughout the synthesis. Finally, mixing an aqueous dispersion (1.5 mL) of the modified core–shell particles with an aqueous dispersion (20 mL) of citrate-stabilized Au nanoparticles (described as Au seeds for clarification in the following contents) resulted in the adsorption of Au seeds on the Fe_3O_4-SiO_2 core–shell particles with the assistance of strong sonication for 10 min. The Fe_3O_4-SiO_2 core–shell particles decorated with Au seeds were separated from the excessive Au seeds with the assistance of an external magnetic field, washed with DI water, and re-dispersed in DI water (1 mL). The Fe_3O_4-SiO_2 core–shell particles decorated with the Au seeds were then coated with a second SiO_2 layer through the similar Stöber method. Carefully controlling the reaction time resulted in that the Au seeds were partially embedded in the silica matrix. The particles were then collected, washed, and re-dispersed in DI water (1 mL) for further use. The entire synthesis was performed at room temperature and in ambient environment.

Overgrowth of Ag on the Au Seeds: The Fe_3O_4-SiO_2 core–shell particles decorated with Au seeds that were synthesized in the previous step had the Au seeds partially exposed to the surrounding environment, enabling the seed-mediated growth of Ag on the Au seeds. In a typical seeded growth reaction, DI water (4 mL), acetonitrile (1 mL), aqueous PVP K12 solution (500 µL, 5 wt%), aqueous sodium citrate solution (1 mL, 0.1 M), aqueous ascorbic acid solution (400 µL, 0.1 M), and aqueous $AgNO_3$ solution (300 µL, 0.01 M) were sequentially added to a 20-mL vial under continuous magnetic stirring to form the growth solution. To the growth solution was injected the dispersion (150 µL) of the composite particles synthesized in the previous step, which quickly triggered the growth of Ag domains on the Au seeds together with a significant color change from brick red to brick blue, then brown, and finally grey brown. The growth of Ag domains lasted 10 min to reach the appropriate size. The resulting Fe_3O_4-SiO_2-Au-Ag composite particles were then separated from the growth solution with the assistance of an external magnetic field. After the particles were washed with water twice, they were re-dispersed in DI water (5 mL) for further use.

Synthesis of Interfaced Dimers Made of Au Nanoparticles (Au NPs) and Bimetallic Nanoshells: The Ag domains in the composite particles synthesized in the previous step could be converted to bimetallic (or alloyed) nanoshells with hollow interiors through the nanoscale galvanic replacement reactions between the Ag domains and appropriate noble metal precursors,[42] leading to the formation of asymmetric, interfaced dimers made of solid Au NPs and bimetallic nanoshells. In a typical synthesis of the Au NP-Au/Ag nanoshell dimers, a dispersion (5 mL) of the Fe_3O_4-SiO_2-Au-Ag composite nanoparticle was first mixed with PVP K15 aqueous solution (1 mL, 5 wt%) in a 20-mL vial. A designed amount of aqueous $HAuCl_4$ solution (0.5 mM) was added drop by drop to the nanoparticle dispersion in a boiled water bath. The fast reaction led to a color change from gray brown to gray black. The particles were collected with the assistance of an external magnetic field and washed with water. The purified particles were then re-dispersed in an aqueous solution of NaOH (5 mL, 0.01 M) and incubated for 1 h to dissolve the SiO_2 layers in the composite nanoparticles and release the Au NP-Au/Ag nanoshell dimers to the solution. The Fe_3O_4 cores can be separated by a magnet and reused for a new cycle of synthesis. The leftover dimers in the solution collected through centrifugation were then washed with DI water twice and re-dispersed in DI water (2 mL) for characterization. For the synthesis of dimers made of solid Au NPs and different nanoshells, different metal precursors were used to react with the Ag domains, for example, Na_2PdCl_4 (0.5 mM) and Na_2PtCl_4 (0.5 mM) aqueous solutions were used for the Au NP-Pd/Ag nanoshell dimers and Au NP-Pt/Ag nanoshell dimers, respectively.

Characterization: A JEOL 2010F(s) transmission electron microscope (TEM) was used to characterize the morphology of the synthesized nanoparticles. To prepare a TEM sample, a drop of aqueous dispersion of nanoparticles was delivered to a carbon-coated copper grid with

the use of a micropipette, followed by drying in a fume hood at room temperature. The TEM images were obtained at 200 kV acceleration voltage. The energy dispersive X-ray (EDX) spectra were collected with an INCA X-ray microanalysis system equipped on the JEOL 2010F(s) microscope. A JSM JEOL 7500F field-emission scanning electron microscope operated at 20 kV under high-vacuum mode was used to record the SEM images. A VARIAN CARY-50 spectrophotometer was used to record the absorption spectra of dispersions of the synthesized nanoparticles. FEI Tecnai F20ST (S)TEM was used for the electron tomography in three dimensional reconstructions of an asymmetric dimer made of a Au NP and a Au/Ag nanoshell and the EDX spectral line scanning across an asymmetric dimer.

Photo-Enhanced Catalysis of Suzuki Coupling Reactions: The as-synthesized interfaced dimers made of Au NPs and Pd/Ag nanoshells that were attached to the Fe_3O_4-SiO_2 colloidal substrates were used for catalyzing Suzuki coupling reactions to estimate the influence of light illumination. The Suzuki coupling reactions between phenylboronic acid and iodobenzene were carried out in 20-mL glass vials in a water bath set at 80 °C. In a typical reaction, phenylboronic acid (0.073 g) was added to ethanol (9 mL) in the presence of iodobenzene (34 μL). The Au NP-Pd/Ag nanoshell dimers on Fe_3O_4-SiO_2 colloids (3 mg) were re-dispersed in aqueous K_2CO_3 solution (1 mL, 0.138 g mL^{-1}) that was then mixed with the previous solution to catalyze the coupling reaction. A 200 W Xe lamp with light intensity of 120 mW cm^{-2} (filtrated with a 10 cm IR water filter and a 420 nm cutoff filter) was used to promote the catalytic performance. The products were extracted with hexane and immediately analyzed with gas chromatography-mass spectrometry (GC-MS, Agilent Technologies 5975C GC/MS). Both the reactions with and without the use of Xe lamp illumination were carried out to study the influence of photo-illumination on the catalytic coupling reactions.

Supporting Information

Supporting Information is available from the Wiley Online Library or from the author.

Acknowledgements

This work was performed at the Center for Nanoscale Materials, a U.S. Department of Energy, Office of Science, Office of Basic Energy Sciences User Facility under Contract No. DE-AC02-06CH11357. Help from Dr. Elena Rozhkova and Dr. Peng Wang in Suzuki coupling reactions are greatly appreciated.

Received: October 17, 2013
Revised: November 11, 2013
Published online: January 20, 2014

[1] J. N. Anker, W. P. Hall, O. Lyandres, N. C. Shah, J. Zhao, R. P. Van Duyne, *Nat. Mater.* **2008**, *7*, 442.
[2] P. K. Jain, X. Huang, I. H. El-Sayed, M. A. El-Sayed, *Acc. Chem. Res.* **2008**, *41*, 1578.
[3] J. M. Campelo, D. Luna, R. Luque, J. M. Marinas, A. A. Romero, *ChemSusChem* **2009**, *2*, 18.
[4] S. T. Selvan, T. T. Y. Tan, D. K. Yi, N. R. Jana, *Langmuir* **2010**, *26*, 11631.
[5] M. Salerno, J. R. Krenn, B. Lamprecht, G. Schider, H. Ditlbacher, N. Felidj, A. Leitner, F. R. Aussenegg, *Opto–Electron. Rev.* **2002**, *10*, 217.
[6] P. K. Jain, X. Huang, I. H. El-Sayed, M. A. El-Sayad, *Plasmonics* **2007**, *2*, 107.
[7] K. A. Willets, R. P. Van Duyne, *Annu. Rev. Phys. Chem.* **2007**, *58*, 267.
[8] C. L. Nehl, J. H. Hafner, *J. Mater. Chem.* **2008**, *18*, 2415.
[9] W. Xiong, D. Sikdar, M. Walsh, K. J. Si, Y. Tang, Y. Chen, R. Mazid, M. Weyland, I. D. Rukhlenko, J. Etheridge, M. Premaratne, X. Li, W. Cheng, *Chem. Commun.* **2013**, *49*, 9630.
[10] P.-P. Fang, A. Jutand, Z.-Q. Tian, C. Amatore, *Angew. Chem. Int. Ed.* **2011**, *50*, 12184.
[11] M. Cargnello, V. V. T. Doan-Nguyen, T. R. Gordon, R. E. Diaz, E. A. Stach, R. J. Gorte, P. Fornasiero, C. B. Murray, *Science* **2013**, *341*, 771.
[12] R. Narayanan, M. A. El-Sayed, *Nano Lett.* **2004**, *4*, 1343.
[13] Y. Bing, H. Liu, L. Zhang, D. Ghosh, J. Zhang, *Chem. Soc. Rev.* **2010**, *39*, 2184.
[14] C. M. Sanchez-Sanchez, J. Solla-Gullon, F. J. Vidal-Iglesias, A. Aldaz, V. Montiel, E. Herrero, *J. Am. Chem. Soc.* **2010**, *132*, 5622.
[15] A. R. Tao, S. Habas, P. Yang, *Small* **2008**, *4*, 310.
[16] X. Lu, M. Rycenga, S. E. Skrabalak, B. Wiley, Y. Xia, *Annu. Rev. Phys. Chem.* **2009**, *60*, 167.
[17] L. M. Liz-Marzan, *Langmuir* **2006**, *22*, 32.
[18] Y. Xia, Y. Xiong, B. Lim, S. E. Skrabalak, *Angew. Chem. Int. Ed.* **2009**, *48*, 60.
[19] C. Sonnichsen, B. M. Reinhard, J. Liphardt, A. P. Alivisatos, *Nat. Biotechnol.* **2005**, *23*, 741.
[20] S.-C. Yang, H. Kobori, C.-L. He, M.-H. Lin, H.-Y. Chen, C. Li, M. Kanehara, T. Teranishi, S. Gwo, *Nano Lett.* **2010**, *10*, 632.
[21] S. Sheikholeslami, Y. W. Jun, P. K. Jain, A. P. Alivisatos, *Nano Lett.* **2010**, *10*, 2655.
[22] G. Chen, Y. Wang, M. Yang, J. Xu, S. J. Goh, M. Pan, H. Chen, *J. Am. Chem. Soc.* **2010**, *132*, 3644.
[23] C. E. Talley, J. B. Jackson, C. Oubre, N. K. Grady, C. W. Hollars, S. M. Lane, T. R. Huser, P. Nordlander, N. J. Halas, *Nano Lett.* **2005**, *5*, 1569.
[24] J. M. Romo-Herrera, R. A. Alvarez-Puebla, L. M. Liz-Marzan, *Nanoscale* **2011**, *3*, 1304.
[25] M. M. Maye, D. Nykypanchuk, M. Cuisinier, D. van der Lelie, O. Gang, *Nat. Mater.* **2009**, *8*, 388.
[26] A. Alivisatos, K. Johnsson, X. Peng, T. Wilson, C. Loweth, M. Bruchez, P. Schultz, *Nature* **1996**, *382*, 609.
[27] S. A. Claridge, A. J. Mastroianni, Y. B. Au, H. W. Liang, C. M. Micheel, J. M. J. Frechet, A. P. Alivisatos, *J. Am. Chem. Soc.* **2008**, *130*, 9598.
[28] J. J. Storhoff, R. Elghanian, R. C. Mucic, C. A. Mirkin, R. L. Letsinger, *J. Am. Chem. Soc.* **1998**, *120*, 1959.
[29] W. Li, P. H. C. Camargo, L. Au, Qiang Zhang, Matthew Rycenga, Y. Xia, *Angew. Chem. Int. Ed.* **2010**, *49*, 164.
[30] X. Wang, G. Li, T. Chen, M. Yang, Z. Zhang, T. Wu, H. Chen, *Nano Lett.* **2008**, *8*, 2643.
[31] B. Wang, B. Li, B. Zhao, C. Y. Li, *J. Am. Chem. Soc.* **2008**, *130*, 11594.
[32] L. Cheng, J. Song, J. Yin, H. Duan, *J. Phys. Chem. Lett.* **2011**, *2*, 2258.
[33] D. J. Kraft, R. Ni, F. Smallenburg, M. Hermes, K. Yoon, D. A. Weitz, A. van Blaaderen, J. Groenewold, M. Dijkstra, W. K. Kegel, *Proc. Natl. Acad. Sci. U.S.A.* **2012**, *109*, 10787.
[34] T. Chen, G. Chen, S. Xing, T. Wu, H. Chen, *Chem. Mater.* **2010**, *22*, 3826.
[35] S. Xing, Y. Feng, Y. Y. Tay, T. Chen, J. Xu, M. Pan, J. He, H. H. Hng, Q. Yan, H. Chen, *J. Am. Chem. Soc.* **2010**, *132*, 9537.
[36] H. Xing, Z. Wang, Z. Xu, N. Y. Wong, Y. Xiang, G. L. Liu, Y. Lu, *ACS Nano* **2012**, *6*, 802.
[37] T. Chen, M. Yang, X. Wang, L. H. Tan, H. Chen, *J. Am. Chem. Soc.* **2008**, *130*, 11858.
[38] Y. Hu, Y. Sun, *J. Am. Chem. Soc.* **2013**, *135*, 2213.
[39] Y. Hu, Y. Sun, *J. Phys. Chem. C* **2012**, *116*, 13329.
[40] Y. Sun, J. J. Foley, S. Peng, Z. Li, S. K. Gray, *Nano Lett.* **2013**, *13*, 3958.

[41] Q. Zhang, I. Lee, J. Ge, F. Zaera, Y. Yin, *Adv. Funct. Mater.* **2010**, *20*, 2201.
[42] Y. Sun, B. Wiley, Z. Y. Li, Y. N. Xia, *J. Am. Chem. Soc.* **2004**, *126*, 9399.
[43] Y. Sun, Y. Xia, *J. Am. Chem. Soc.* **2004**, *126*, 3892.
[44] Y. Sun, B. Mayers, Y. N. Xia, *Adv. Mater.* **2003**, *15*, 641.
[45] S.-J. Kim, S.-D. Oh, S. Lee, S.-H. Choi, *J. Ind. Eng. Chem.* **2008**, *14*, 449.
[46] S. W. Kim, M. Kim, W. Y. Lee, T. Hyeon, *J. Am. Chem. Soc.* **2002**, *124*, 7642.
[47] R. Narayanan, *Molecules* **2010**, *15*, 2124.
[48] H. Zhu, X. Ke, X. Yang, S. Sarina, H. Liu, *Angew. Chem. Int. Ed.* **2010**, *49*, 9657.
[49] X. Chen, H.-Y. Zhu, J.-C. Zhao, Z.-T. Zheng, X.-P. Gao, *Angew. Chem. Int. Ed.* **2008**, *47*, 5353.
[50] J. R. Adleman, D. A. Boyd, D. G. Goodwin, D. Psaltis, *Nano Lett.* **2009**, *9*, 4417.
[51] C.-W. Yen, M. A. El-Sayed, *J. Phys. Chem. C* **2009**, *113*, 19585.
[52] W. H. Hung, M. Aykol, D. Valley, W. Hou, S. B. Cronin, *Nano Lett.* **2010**, *10*, 1314.
[53] F. Wang, C. Li, H. Chen, R. Jiang, L.-D. Sun, Q. Li, J. Wang, J. C. Yu, C.-H. Yan, *J. Am. Chem. Soc.* **2013**, *135*, 5588.
[54] J. Ye, L. Lagae, G. Maes, P. Van Dorpe, *J. Mater. Chem.* **2011**, *21*, 14394.
[55] J. Ge, Y. Hu, M. Biasini, W. P. Beyermann, Y. Yin, *Angew. Chem. Int. Ed.* **2007**, *46*, 4342.
[56] J. Ge, Y. Yin, *Adv. Mater.* **2008**, *20*, 3485.